Collective dynamics in liquid cesium near the melting point

T. Bodensteiner, Chr. Morkel, and W. Gläser
Physik Department, Technische Universität München, D-8046 Garching, Germany

B. Dorner
Institut Laue-Langevin, F-38042 Grenoble CEDEX, France

(Received 11 June 1991)

The coherent dynamic structure factor $S(Q,\omega)$ of liquid Cs has been measured by inelastic neutron scattering near the melting point at 308 K. Using triple-axis spectrometers at the Institut Laue-Langevin in Grenoble and at the Forschungs-Reaktor München the scattering law was determined for energy transfers $\hbar\omega$ from -2 to 10 meV and for momentum transfers $\hbar Q$ between 0.2 and 2.55 Å^{-1}. The measurement has been corrected for all significant effects, including multiple and incoherent scattering as well as resolution broadening. In this paper we present mainly experimental results including a table of the measured scattering law. The analysis of the dispersion relation and the full width at half maximum of the longitudinal current correlation function $J_1(Q,\omega)$ reveals an anomalous dispersion due to shear relaxation in the liquid. In the vicinity of the structure-factor maximum the measured half-width of the coherent central peak of $S(Q,\omega)$ confirms recent theoretical assumptions of a collective-diffusion-like structural relaxation process in dense liquids near the melting point.

PACS number(s): 62.15.+i, 67.40.Fd

I. INTRODUCTION

Though the existence of collective modes in liquids at atomic distances has been shown long ago by the pioneering scattering experiments in liquid lead [1], argon [2], and rubidium [3], only a few neutron-scattering experiments have been published that allow a detailed analysis of the underlying processes of collective dynamics. The development of new theoretical models was mainly based on molecular-dynamics calculations on argon [4] and rubidium [5].

After a period of progress mainly in the understanding of single-particle phenomena in liquids, in recent years new interest in collective phenomena has arisen from molecular-dynamics studies of hard spheres [6] and precise scattering experiments on argon [7], neon [8], and lead [9].

It has been known for a long time that liquid metals, unlike dense Lennard-Jones systems, show collective behavior in the form of distinct side peaks in the excitation spectra far outside the hydrodynamic region. Thus these fluids are particularly suitable for an investigation of collective dynamics in the liquid state. Moreover, cesium is one of the last representatives of simple liquid metals for which no inelastic-neutron-scattering experiments have been published up to now.

II. BASIC FORMULAS

The double differential cross section $d^2\sigma/d\Omega d\omega$ obtainable from inelastic-neutron-scattering experiments by trivial transformations, is directly related to the dynamic structure factor $S(Q,\omega)$ which is the double Fourier transform of the particle-density correlation function. In the case of a nonzero incoherent-scattering cross section of the sample, the incoherent scattering law $S_s(Q,\omega)$ has to be included in the correction of the experimental data. $d^2\sigma/d\Omega d\omega$ can then be written as

$$\frac{k_i}{k_f}\frac{d^2\sigma}{d\Omega d\omega}=\left[\frac{\sigma_c}{4\pi}S(Q,\omega)+\frac{\sigma_i}{4\pi}S_s(Q,\omega)\right]\times e^{\hbar\omega/2k_BT}e^{-\hbar^2Q^2/8Mk_BT}, \tag{1}$$

where k_i is the initial wave vector and k_f the final wave vector of the neutron. $\hbar Q$ is the momentum transfer, $\hbar\omega$ is the energy transfer, σ_c and σ_i are the coherent and incoherent nuclear cross sections of the scatterer with mass M. The exponential factors in Eq. (1), where k_B denotes the Boltzmann constant and T the temperature, are necessary corrections for detailed balance and recoil to obtain the scattering law in the symmetrized classical form.

The first two even moments of $S(Q,\omega)$, which are defined generally by

$$\langle\omega^n\rangle=\int_{-\infty}^{\infty}\omega^nS(Q,\omega)d\omega \tag{2}$$

in the classical treatment, are known exactly and are therefore useful for testing the reliability of the experimental data and are given by

$$\langle\omega^0\rangle=S(Q),\quad \langle\omega^2\rangle=v_0^2Q^2,\quad v_0^2=\frac{k_BT}{M} \tag{3}$$

where $S(Q)$ denotes the structure factor of the liquid.

As an expression for the fourth moment, necessary for model calculations in Sec. IV, we used in this work the approximation of Hubbard and Beeby [10],

$$\langle\omega^4\rangle=\langle\omega^2\rangle\left[3\langle\omega^2\rangle+\omega_E^2\left[1-\frac{3\sin(QR_0)}{QR_0}-\frac{6\cos(QR_0)}{(QR_0)^2}+\frac{6\sin(QR_0)}{(QR_0)^3}\right]\right], \quad (4)$$

with ω_E the Einstein frequency and R_0 the maximum of $g(r)\partial^2u(r)/\partial r^2$ as parameters of the liquid.

Another important correlation function in the theory of liquids is the so-called current correlation function. Its longitudinal part, which is easily obtained from the scattering law, is very useful for the description of the dynamics in a liquid:

$$J_1(Q,\omega)=\frac{\omega^2}{Q^2}S(Q,\omega)\ . \quad (5)$$

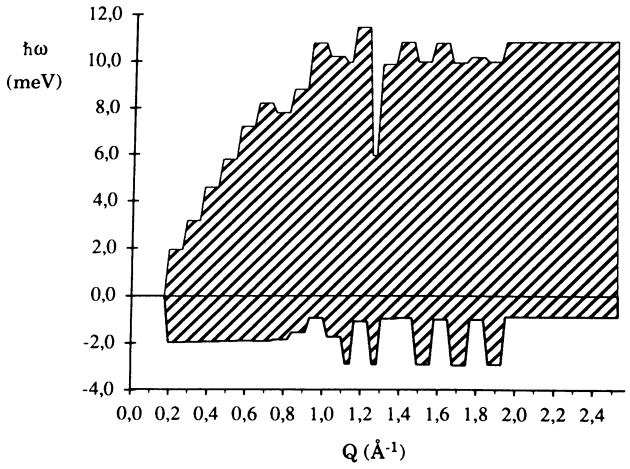

FIG. 1. Kinematic region of the experiments.

III. EXPERIMENTAL DETAILS

The experiment was performed at the triple-axis spectrometers IN8 at the Institut Laue-Langevin (ILL) in Grenoble (measurements I and II) and at F3 at the Forschungs-Reaktor München (FRM) in Munich (measurement III) (see Table I). All measurements were obtained at constant Q while the analyzer energy was kept fixed to allow an easy normalization of the data on an absolute scale [11]. The instruments are described in detail elsewhere [12,13].

The IN8 instrument was operated with an outgoing neutron energy of 14.66 meV selected from a pyrolytic graphite PG 002 monochromator crystal. To suppress higher-order contamination of the scattered intensity a $\lambda/2$ filter was installed in front of the analyzer crystal. The sensitivity of the fission chamber in the incident beam to higher-order neutrons has been taken into account in the data evaluation yielding an absolute normalization of the scattering law. The experiment at the F3 spectrometer was conducted with a neutron energy of 22.5 MeV from a Cu 111 monochromator operated without a $\lambda/2$ filter.

The energy resolution for elastically scattered neutrons was obtained from vanadium measurements, which were also used for calibrating the spectrometers. The resolution full width at half maximum (FWHM) was 0.68 meV for measurement I, which was performed at low Q with a helium-filled box around the flight path of the neutron for reduction of air scattering, 0.72 meV for measurement II at high Q and 0.45 meV for measurement III, which were both performed with a vacuum vessel around the sample. The kinematic region covered by the experiment is shown in Fig. 1 and the measured scans at constant Q vector are listed for all measurements in Table I. The momentum resolution was calculated to be better than 0.05 Å^{-1} and was therefore not considered in data reduction.

The sample, liquid cesium of high purity (99.9%), was held in a cylindrical tube of aluminum of 22.0-mm inner diameter and 0.2-mm wall thickness. In these dimensions the scattered intensity of the sample can be calculated from the total cross section to be about 2.6%, with a multiple scattering portion of about 0.8% of the scattered intensity [14] [$\sigma_c=3.69$ b, $\sigma_i=0.22$ b (see Sec. IV C), $\sigma_a=29.0$ b ($\lambda=1.8$ Å)] [15]. The thermophysical data of liquid cesium as used for data reduction (Sec. IV) and representation of the scattering law (Sec. V) are given in Table II.

Due to the low melting temperature of cesium ($T_M=301.6$ K) it was easy to obtain a constant sample temperature of 308 K by heating the ends of the tube during the measurements which lasted 8.5 days at IN8 and 120 days at F3.

IV. DATA REDUCTION

A. Normalization of data

Because of a lack of data-reduction programs for the evaluation of triple-axis spectrometer experiments into absolute units, a complete program had to be developed. A full description can be found in Ref. [18]; here only a brief summary of the procedure will be given.

Using a fission chamber with a $1/v$ dependency of the efficiency as a monitor counter the double differential cross section $d^2\sigma/d\Omega d\omega$ [see Eq. (1)] can be written [11]

TABLE I. Covered momentum transfers and resolution (FWHM) in all measurements.

Measurement	Momentum transfer (Å^{-1}) Cesium	Vanadium	Resolution (meV)
I	0.20 0.30 0.40 0.50 0.60 0.70 0.80 0.90 1.10 1.20 1.30	0.30 0.60 0.90	0.68
II	1.00 1.30 1.40 1.60 1.80 2.00 2.20 2.40 2.55	1.60 2.20	0.72
III	1.15 1.25 1.50 1.70 1.90	1.25 1.70	0.45

TABLE II. Thermodynamic and transport properties of liquid cesium at 308 K.

			Ref.
Density	ρ	1.831 g/cm^3	[16]
Number density	n	0.830×10^{22} cm^{-3}	[16]
Melting point	T_M	301.6 K	[16]
Adiabatic sound velocity	v_s	965.1 m/s	[16]
Thermal velocity	v_0	138.2 m/s	[Eq. (3)]
Specific heat at constant pressure	c_p	0.236 J/(gK)	[16]
c_p/c_v	γ	1.102	[16]
Isothermal compressibility	χ_T	0.658×10^{-3} MPa^{-1}	[16]
Macroscopic heat conductivity	κ	18.4 W/mK	[16]
Phonon contribution of κ	κ	9.8×10^{-2} W/mK	[see Sec. IV]
Self-diffusion constant	D	2.35×10^{-5} cm^2/s	[16]
Heat diffusion constant	D_H	3.0×10^{-3} cm^2/s	[see Sec. IV]
Viscosity	η	0.70×10^{-3} Pa s	[17]
Bulk viscosity	η_B	2.04×10^{-3} Pa s	[17]
Longitudinal viscosity	η_l	2.97×10^{-3} Pa s	[Eq. (8)]
Einstein frequency	ω_E	4.12×10^{12} s^{-1}	[18,19]
Hard-core diameter	σ	4.80 Å	[18,20]

$$\frac{k_i}{k_f}\frac{d^2\sigma}{d\Omega d\omega}=\frac{k_i}{k_f}\frac{r}{k_f^3 c(k_f)N_S\Delta\Omega}\ , \tag{6}$$

where r denotes the measured rate normalized by the monitor counts corrected for higher-order intensity, c is a spectrometer constant depending only on k_f, $\Delta\Omega$ is the solid angle of the detector, and N_S is the number of scatterers in the beam.

So if k_f is held constant during the measurement, the calibration constant $c(k_f)$ is easily obtained from the elastic scattering of vanadium, which is given by

$$(d\sigma/d\Omega)_{\rm el}=\sigma_s/4\pi e^{-aQ^2}\ , \tag{7}$$

where the scattering cross section σ_s is 5.18 b [15] and the temperature factor a is 0.572×10^{-2} Å^2 at room temperature. After correction for absorption in the vanadium sample, the data were integrated over the elastic peak and compared to Eq. (7). The resulting factors were then used as normalization constant for the cesium measurement.

B. Multiple scattering and absorption correction

For the calculation of accurate data from neutron-scattering experiments it is essential to correct for multiple scattering in the sample. Even when the total contribution to the scattered intensity is only about 1%, as in our case, it turned out that especially at low momentum transfers and at high-energy transfers the multiple scattering contribution was up to 50% of the sample scattering. As multiple scattering cannot be measured experimentally, a Monte Carlo program, developed by Copley *et al.* [21], was used for calculating the multiple-scattering contribution. Though it was written for time-of-flight geometry, it could be shown to be usable as well for the triple axis geometry in our case with minor modifications [18]. The parameters of the programlike flight path and time resolution were chosen such that the results of a vanadium simulation gave results as close as possible to the experiment. As model input for the cesium simulation, single-relaxation-time models for $S(Q,\omega)$ and $S_s(Q,\omega)$ were used [22,23], which were fitted to the

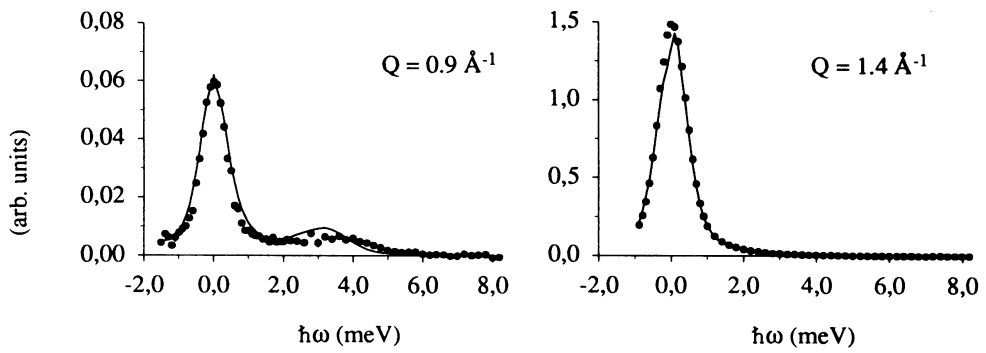

FIG. 2. Comparison between measured scattering law after data correction (circles) and simulated Cs spectra of MSCAT (solid line). (For data reduction we used only the multiple-scattering spectra of MSCAT.)

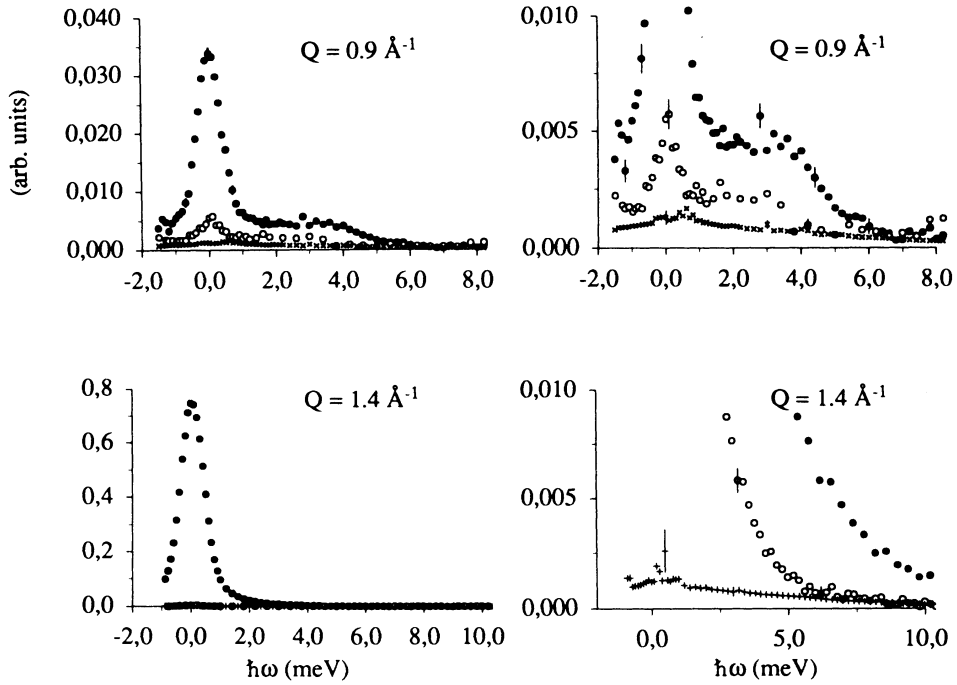

FIG. 3. Comparison between counting rates of cesium (solid circles), empty container (open circles), and simulated multiple-scattering spectra (crosses). The right figures are magnifications of the left ones.

experimental data in the measured kinematic region.

As the simulation yields the multiple- as well as the single-scattering contribution for both the coherent- and incoherent-scattering law, the computation could be checked against the measurement and gave a very good agreement (Fig. 2). As we used only the multiple-scattering contribution, which is rather insensitive to the exact form of the scattering law due to the large half width at half maximum (half-width) and independence of momentum transfer, we consider the simulation (120 000 neutrons) to be a good approximation to the experimental situation. To avoid too much influence of the input model we did not use the factor method [21] but substracted the properly normalized multiple scattering spectra directly from the experimental data. Figure 3 shows the contributions of multiple and container scattering to the results for two spectra, while in Fig. 4 the integral contributions for low Q are shown.

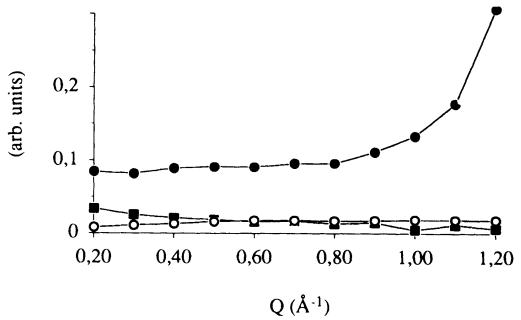

FIG. 4. Comparison between integrated intensities of cesium (solid circles), empty container (open circles), and multiple-scattering contribution (squares).

After this self-absorption and background corrections for cesium as well as for vanadium were performed with the formalism of Paalman and Pings [24], where an energy- and momentum-transfer-dependent effective cross section is calculated by integrating over different flight paths in the sample.

C. Incoherent scattering

Though the incoherent scattering cross section of cesium is only a small fraction of the total cross section, it leads to a considerable contribution in the spectra at low Q and has to be taken into account. We used a single relaxation time model [23], which was shown to work reasonably well at low Q [25], to calculate the incoherent contribution. It had the advantage of all parameters to be known without fitting.

Because of the good separation of the coherent and incoherent part in the spectra, due to a two-order-of-magnitude difference between the diffusion and thermal diffusion constants, which determine the half-width of the spectra at low Q, a quite accurate estimate of the incoherent cross section could be evaluated from the data which was found to be $\sigma_i = 0.33 \pm 0.05$ b [18]. A data evaluation with the newest value found in literature ($\sigma_i = 0.22 \pm 0.05$ b [15]) did not yield reasonable results for the half-width of the coherent scattering law.

D. Resolution correction

An essential correction for getting accurate results for $S(Q,\omega)$ at low-energy transfers is a resolution correction. As a numerical deconvolution of nonperiodic data does

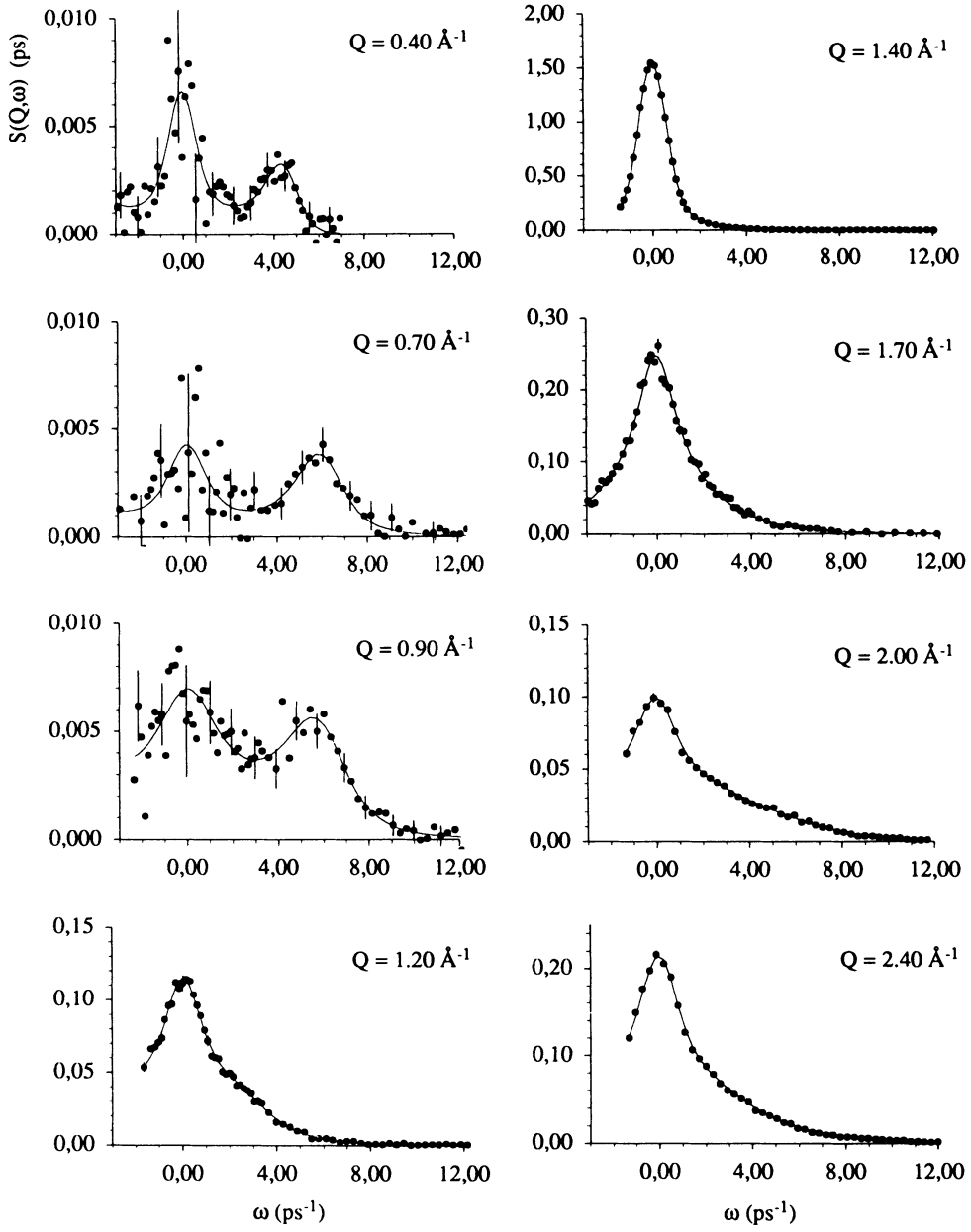

FIG. 5. Selected spectra of the coherent dynamic structure factor $S(Q,\omega)$. Circles, experimental $S(Q,\omega)$; solid line, parametrized form of the experimental data set (see text) folded with the resolution function.

not yield reliable results, we used another method in this work, which depends on the fact, that the principal features of the scattering law—such as dispersive sidepeaks and the central thermal diffusion peak—are well known from theory.

Thus assuming appropriate models to be not so far from reality, we used the least-square-fit method to fit a theory function, folded with the experimental resolution function to the data, leaving free at least six parameters to ensure a minimal χ^2. The analytical function, calculated with the fitted parameters was then believed to give the unfolded experimental values. Tests of this procedure with known functions gave reliable results [18]. The resolution function was evaluated from the vanadium data and was well described by a Gaussian (see Table I).

To get a measure for the involved errors, we used two models as fit functions. One was a coherent single relaxation time model [22]; the other model used was a memory function ansatz with two relaxation times [26]. It turned out that the differences of the two fits were everywhere smaller than the statistical errors of the experiment. In Fig. 5 we show some representative results of the symmetrized dynamic scattering function $S(Q,\omega)$ without resolution correction to show the excellent agreement of the parametrized representation of the data (full line) with the experimental values (circles).

V. RESULTS

A. Dynamic scattering law $S(Q,\omega)$

For all measured wave numbers Q the energy spectra of the symmetrized dynamic scattering law $S(Q,\omega)$ of liquid cesium at 308 K are shown in resolution corrected form in Fig. 6. In Table III we present representative numerical results both with and without resolution correction. The errors given in this table are valid only for data without resolution correction. They are interpolated from the experimental errors, which take into account the error propagation of the statistical errors of sample and container measurements, statistical errors of multiple-scattering simulation, and an estimate of the incoherent scattering correction. The errors for the resolution corrected form cannot be derived by the correction method. The differences between the two fitting models are much smaller than the experimental errors. It can thus be concluded that the experimental errors are also a good approximation of the resolution corrected values.

The large errors of the central line at low Q (<0.6 Å^{-1}) are due to the large incoherent and background correction which amounts to 90% of the total scattered

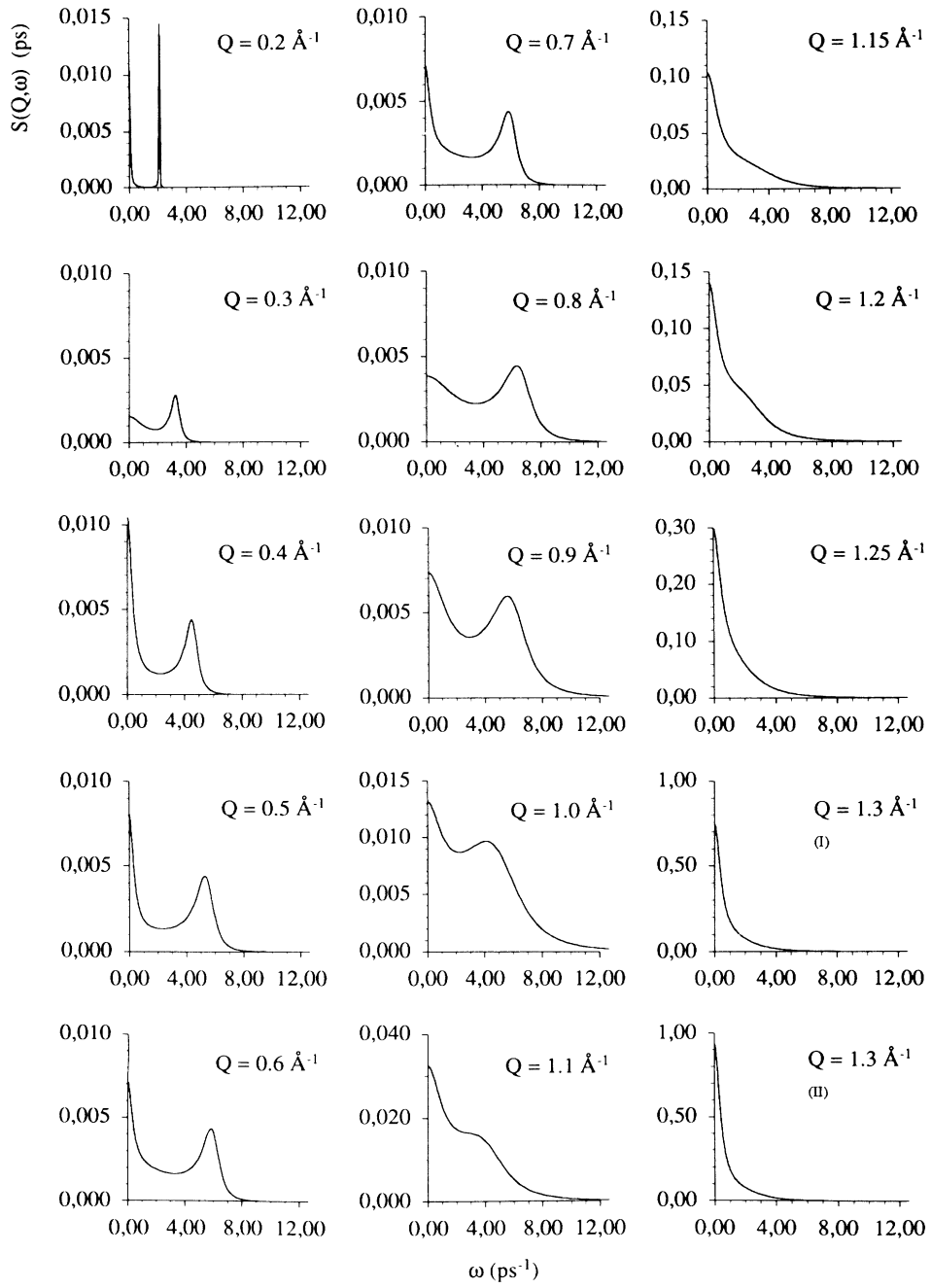

FIG. 6. Dynamic structure factor $S(Q,\omega)$ of liquid cesium at 308 K in resolution corrected form (see Table III).

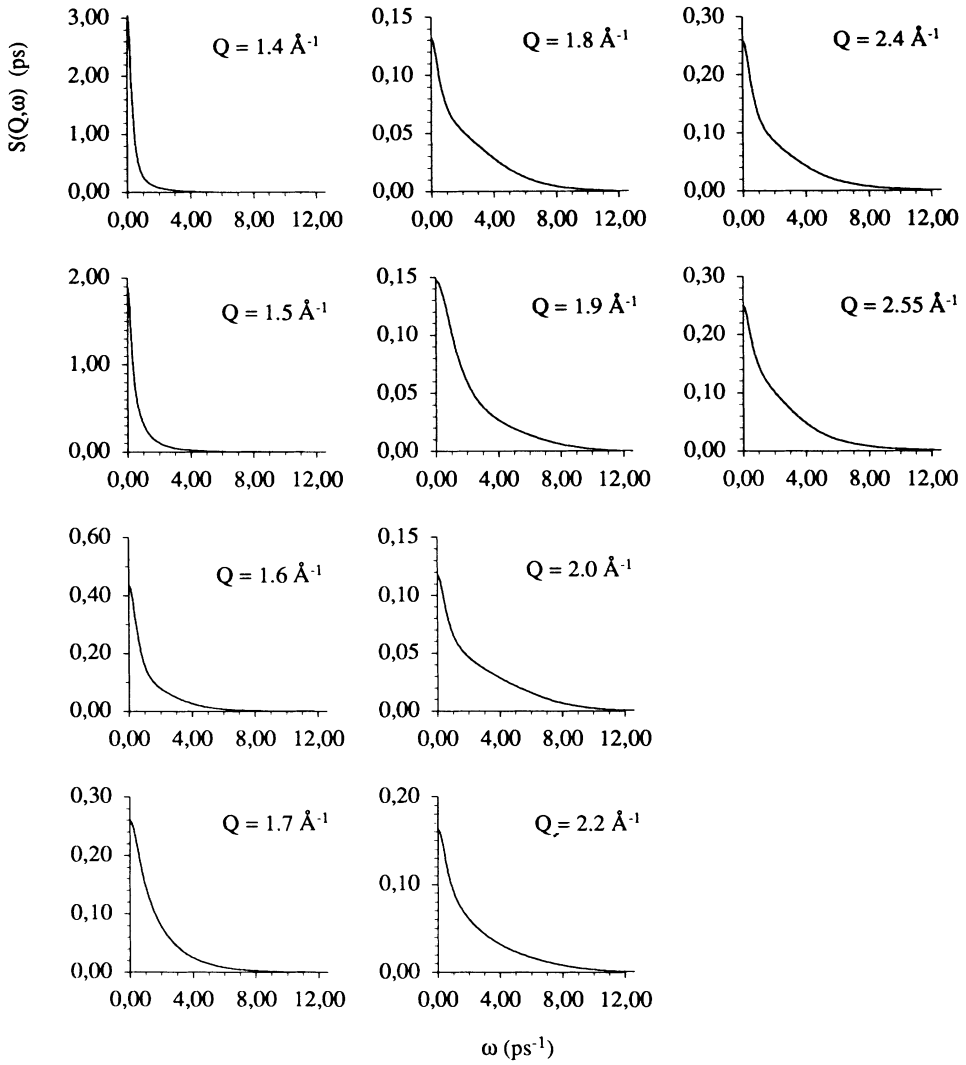

FIG. 6. (*Continued*).

intensity at the smallest momentum transfers. The values of the inelastic peaks and of the central line at higher Q are rather insensitive to these corrections. So the main results presented in this paper are not affected by these corrections.

A careful inspection of the series of scattering laws (Fig. 6) reveals small differences between measurements I and II on the one hand and experiment III on the other hand (see Table I). This appears at least partly due to the different spectrometers used. As mentioned above series III (FRM München) was measured with improved resolution but without a $\lambda/2$ filter, which made it impossible to correct for the obviously small effect of second-order contamination in series III. A $\lambda/2$ filter for the FRM triple axis spectrometer is under construction now.

The values of the peak width and height of the central peak of $S(Q,\omega)$ were easily obtained from the resolution corrected data set. The peak heights $S(Q,0)$ are related to the static longitudinal viscosity $\eta_l(Q)$ by the following equation, derived from generalized hydrodynamics [27]

$$\eta_l(Q)=\pi\rho v_0^2\frac{S(Q,0)}{S(Q)^2},\quad \lim_{Q\to 0}\eta_l(Q)=\tfrac{4}{3}\eta+\eta_B\ , \tag{8}$$

where η and η_B are the macroscopic shear viscosity and bulk viscosity, respectively, and ρ is the density. As shown in Fig. 7, $\eta_l(Q)$ for liquid cesium is a monotonically decreasing function like η_l of Lennard-Jones systems [28]. A comparison of $\eta_l(Q)$ with simple viscoelastic theory (full line in Fig. 7) reveals nearly quantitative agreement in the region beyond Q_0—the position of the structure factor maximum. Viscoelastic theory describes the longitudinal viscosity as

$$\eta_l(Q)=\tfrac{4}{3}G(Q)\tau(Q)\ , \tag{9}$$

neglecting bulk viscosity. $G(Q)$ is the well-known shear modulus of the liquid [29] and $\tau(Q)$ is a Q-dependent relaxation time, which is calculated here with the interpola-

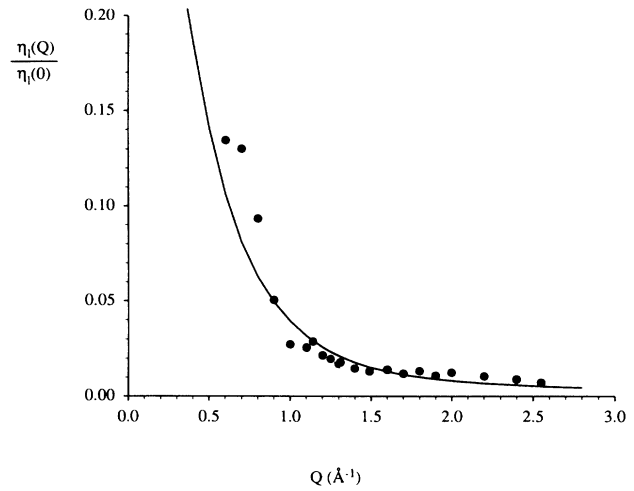

FIG. 7. Reduced static longitudinal viscosity $\eta_l(Q)$ (solid circles). Solid line, viscoelastic theory.

tion formula of Akcazu and Daniels [30].

Not much is known about the Q dependence of the bulk viscosity η_B, but it can be conjectured that the contribution of η_B to $\eta_l(Q)$ is negligible beyond Q_0. It is interesting to note that in liquid lead near the melting point a pronounced peak in $\eta_l(Q)$ beyond Q_0 was found [31]. As bulk viscosity is closely related to local microscopic structure the different findings for cesium and lead may reflect a difference between a simple liquid metal and a polyvalent one.

The peak width of the central line is a measure for viscoelastic relaxation time constants in a liquid. In the hydrodynamic limit the half-width is proportional to $D_H Q^2$, where D_H is the thermal diffusion constant, while it is proportional to $v_0 Q$ in the free-streaming limit. The interesting transition regime which was covered by the experiment is shown in Fig. 8.

Following recent theoretical results the so-called de Gennes minimum of the coherent half-width $\omega_{1/2}(Q)$ in the vicinity of the structure factor maximum at $Q_0=1.42$ Å^{-1} is given by [32]

$$\omega_{1/2}(Q)=[D_E Q^2/S(Q)]d(Q),$$
$$d(Q)=[1-j_0(Q\sigma)+2j_2(Q\sigma)]^{-1}, \tag{10}$$

with the Enskog self-diffusion coefficient D_E, the hard-sphere diameter σ, and the spherical Bessel functions j_l of order l. Thus the main contribution to the scattering law near Q_0 comes from generalized heat fluctuations which show dramatically longer relaxation times near Q_0 in dense liquids. The half-widths $\omega_{1/2}(Q)$ determined from the central line of the resolution corrected scattering law (cf. Table III) are plotted in Fig. 8. The dashed line shows a fit to Eq. (10) in the Q range from 1.2 to 1.8 Å^{-1}, where the central half-widths are not affected by the sidepeaks. This fit yields $D_E^*=(2.6\pm0.1)\times10^{-5}$ cm^2/s compared with $D_E=2.83\times10^{-5}$cm^2/s from the Enskog theory. The hard-sphere diameter kept fixed in this fit was determined independently to $\sigma=4.80\pm0.02$ Å [18].

The de Gennes minimum can thus be understood as a collective-diffusion-like slow structural relaxation process near Q_0 [32] described by an essentially hydrodynamic behavior, as the structural relaxation time $\tau=\omega_{1/2}^{-1}(Q)$ again becomes large on the Enskog time scale τ_E. In contrast to this the validity of the hydrodynamic description of the half-width for small Q ends far below the region covered by the experiment (solid line).

B. Frequency moments

By numerical integration the first two even moments were obtained from the experimental data set, integrating only over the frequency region covered by the measurement. The cutoff error was ignored because of the half-width of the spectra being much smaller than the maximum measured frequency (Fig. 1).

The zeroth moment, the static structure factor $S(Q)$ is shown in Fig. 9. It is in an excellent agreement with an x-ray study performed at 303 K (solid line) [16].

Because of the small counting rates and the large corrections due to background and multiple scattering at high frequencies the higher moments could not be determined accurately. In Fig. 10 the ratio is shown between experimental and theoretical second moment. It is no-

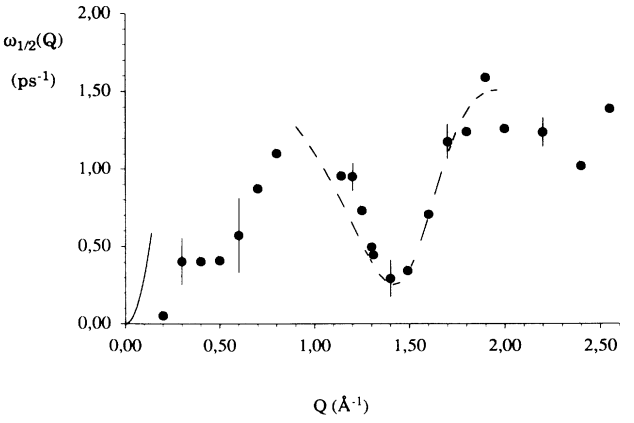

FIG. 8. Central half-widths $\omega_{1/2}(Q)$ of $S(Q,\omega)$ (solid circles). Dashed line, fit of Eq. (10); solid line, hydrodynamic limit.

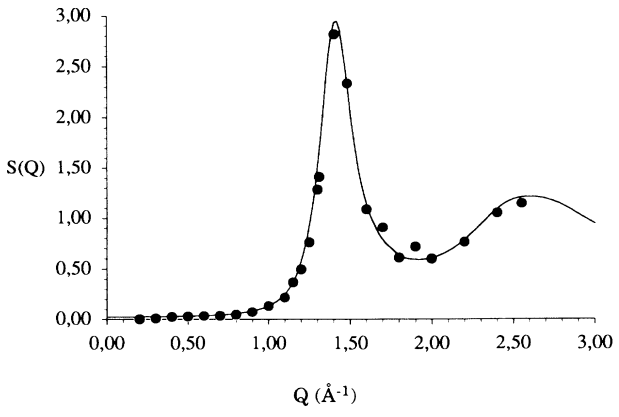

FIG. 9. Experimentally determined static structure factor $S(Q)$ (circles). Solid line, x-ray measurement at 303 K [16].

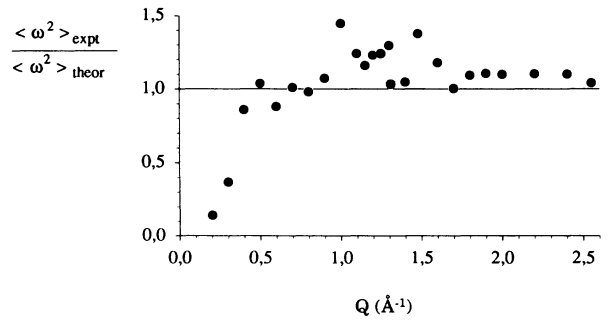

FIG. 10. Ratio between experimental and theoretical second frequency moment of $S(Q,\omega)$.

ticed that the experimental second moment is systematically too large in the region where $S(Q,\omega)$ itself is narrow in frequency. Hence the high ω tails of the scattering function seem to be still contaminated by background or multiple-scattering intensity. Here the way of a triple-axis spectrometer measuring the data set step by step makes it difficult to correct for time-dependent background caused for example by neighboring spectrometers.

C. Longitudinal current correlation function and collective modes

By means of Eq. (5) the frequency spectra of the longitudinal current correlation function $J_l(Q,\omega)$ were ob-

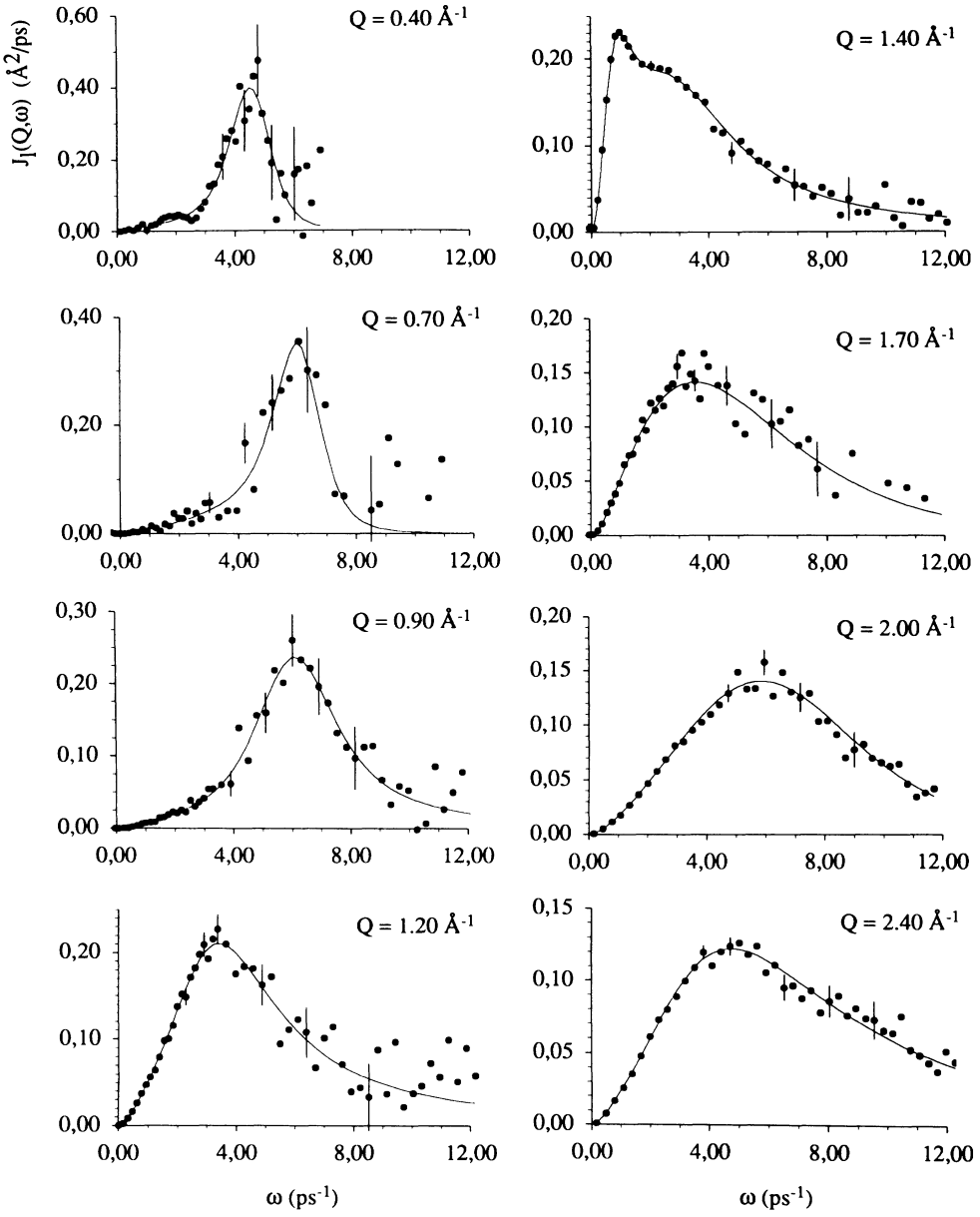

FIG. 11. Selected spectra of the longitudinal current correlation function $J_l(Q,\omega)$. Circles, calculated from experimentally determined $S(Q,\omega)$; solid line, calculated from the parametrized form and folded with the resolution function.

tained from the experimental data as well as from the parametrized form (solid line) as it is shown for some representative spectra in Fig. 11. The resolution corrected data set was used to calculate numerically peak positions (positions of maximum) and peak widths of $J_l(Q,\omega)$. They do not differ significantly from the noncorrected set and are therefore not shown separately.

In contrast to particle-density fluctuations, whose dispersion relation cannot be derived from the spectra beyond a special wave vector without theoretical models, the dispersion relation of $J_l(Q,\omega)$ which gives a measure for correlated current density fluctuations, is determined by the peak position of $J_l(Q,\omega)$ and is defined over the whole Q range. In Fig. 12 we show the dispersion relation ω_m^l of $J_l(Q,\omega)$. From the low-Q slope of the dispersion a clear enhancement can be seen over the acoustic sound velocity $v_s=965$ m/s for liquid Cs at 308 K (dashed line), which is the hydrodynamic limit of ω_m^l as well as for the dispersion of particle density fluctuations [33].

We consider this to be due to the onset of shear relaxations for frequencies above τ_M^{-1}, where τ_M is the Maxwell relaxation time which can be estimated to be $\tau_M=0.87$ ps [26]. This viscoelastic effect results in a shift of the phonon peak to larger ω, thus leading to a positive anomalous dispersion of the collective modes. The corresponding high frequency sound speed c_∞ is given by

$$c_\infty(Q)=\left\{\frac{1}{\rho}\left[\tfrac{4}{3}G_\infty(Q)+K_\infty(Q)\right]\right\}^{1/2} \tag{11}$$

with the wave-vector-dependent shear and bulk moduli $G_\infty(Q)$ and $K_\infty(Q)$.

In the limit $Q\to 0$, $c_\infty(Q)$ can be approximated by [34]

$$c_\infty(0)=(3v_0^2+\tfrac{3}{10}\omega_E^2R_0^2)^{1/2}\ , \tag{12}$$

which gives $c_\infty(0)=1061$ m/s (full line) in good agreement with the experimental data (Fig. 13). A more detailed study of this effect is given elsewhere [35]. By the equation

$$c_\infty(0)=\sqrt{3G/\rho}\ , \tag{13}$$

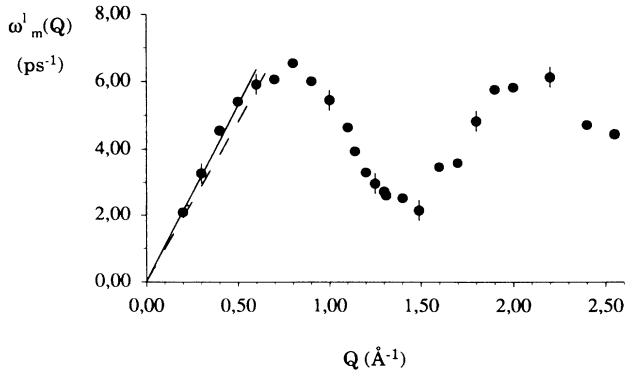

FIG. 12. Dispersion relation $\omega_m^l(Q)$ of the longitudinal current correlation function $J_l(Q,\omega)$. Dashed line, adiabatic sound velocity $c_s=965$ m/s; solid line, $c_\infty=1061$ m/s.

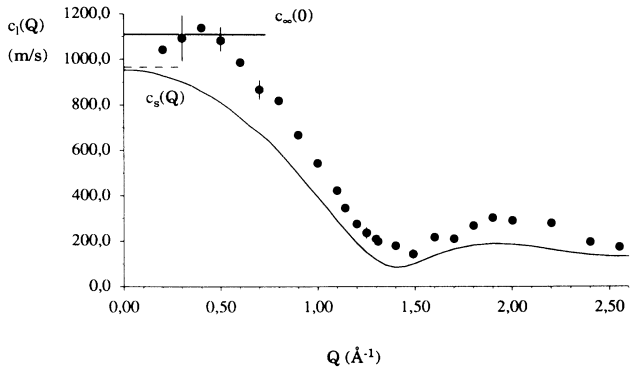

FIG. 13. Sound velocity $c_l(Q)=\omega_m^l(Q)/Q$ determined from the longitudinal current correlation function $J_l(Q,\omega)$. Dashed line, adiabatic sound velocity $v_s=965.1$ m/s; solid lines, high- and low-frequency limit of the sound velocity $c_\infty(0)$ and $c_s(Q)$, respectively.

the shear modulus G of the liquid can be determined from the experiment to $G=(7.67\pm0.95)\times10^9$ g/cm s^2.

From the resolution corrected data set the half-widths $\Delta\omega_m^l$ of $J_l(Q,\omega)$ were easily obtained, and are shown in Fig. 14. The region of nearly linear increase extends from the lowest measured Q far beyond the first structure factor maximum. As can be seen from the solid-line hydrodynamics widely overestimate the half-widths of the sidepeaks as it is the case for the central line width too (Fig. 8).

The interesting question of the existence of nonoverdamped collective particle density modes near and beyond Q_0 can only be answered with a more detailed analysis. But obviously collective excitations exist, showing up as a shoulder in $S(Q,\omega)$, up to at least 1.2 Å^{-1}, which means 85% of Q_0. Thus definitely nonoverdamped collective modes are observed in liquid cesium further than they have been seen before in the scattering law of a liquid.

VI. CONCLUSIONS

We report a neutron-scattering experiment on liquid cesium at a temperature of 308 K as representative of a

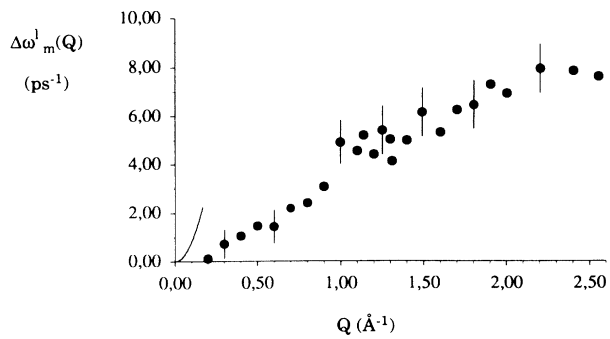

FIG. 14. Full half-widths $\Delta\omega_m^l(Q)$ of the longitudinal current correlation function $J_l(Q,\omega)$. Solid line, hydrodynamic limit.

simple liquid metal near the melting point. After careful corrections for all known experimental effects, the coherent scattering law $S(Q,\omega)$ and the longitudinal current correlation function $J_l(Q,\omega)$ of liquid Cs are determined in a wave number range $0.2 \leq Q \leq 2.55$ Å^{-1}. The accuracy of the data allows quantitative tests of kinetic and mode-coupling theories in the regime beyond the hydrodynamic limit.

The existence of collective density fluctuations can be observed as sidepeaks in $S(Q,\omega)$ up to $Q = 1.2$ Å^{-1}, which means up to 85% of the position of the structure factor maximum at Q_0. An anomalous dispersion of the collective modes is observed which is ascribed to the onset of shear relaxation in the liquid for frequencies above τ_M^{-1}, with τ_M the Maxwell relaxation time. In this frequency region sound propagation is found to be mainly determined by elastic constants—the shear modulus of the liquid is evaluated from the experimental data—rather than by compressibility as in hydrodynamics. Moreover, the damping of these modes is shown to increase only linearly in the Q region covered in the experiment. This also indicates clearly a nonhydrodynamic sound propagation and seems to apply especially to liquid metals, as it is not known from Lennard-Jones systems. The obviously small damping of collective modes in liquid metals raises the question of nonoverdamped modes at Q values beyond Q_0. The interpretation of the shoulders showing up in the experimental data above $Q = 1.8$ Å^{-1}, however, needs further experimental attention and discussion.

The longitudinal viscosity $\eta_l(Q)$ is evaluated showing a decrease of two orders of magnitude from the hydrodynamic region to Q_0. It is concluded that in simple liquid metals the bulk viscosity η_b contributes to $\eta_l(Q)$ only for $Q < Q_0$ in contrast to polyvalent metals such as liquid lead. A clear separation of $\eta_l(Q)$ into bulk and shear viscosity might be interesting, but seems to be possible only in a molecular dynamics simulation study.

The collective dynamic near Q_0 has been studied in more detail and is found to be governed by a cooperative-diffusion-like slow density relaxation according to recently developed concepts of collective dynamics in dense systems [36].

As all these features—anomalous sound dispersion, nonhydrodynamic sound damping, and dynamical slowing down near Q_0—resemble those of a glass forming liquid, it is concluded that these dynamic properties of a liquid metal near the melting point can be viewed as a precursor to the solidification.

ACKNOWLEDGMENTS

We gratefully acknowledge the assistance of the workshop of the Forschungs-Reaktor München and the staff of the Institut Laue-Langevin (Grenoble) with the preparation and performance of the experiments. We also thank Dr. P. Müller and Dr. P. Verkerk for help with the experiment and the MSCAT Program respectively. This work was supported by the German Bundesministerium für Forschung und Technologie.

[1] B. Dorner, T. Plesser, and H. Stiller, Disc. Faraday Soc. **43**, 160 (1967), S. J. Cocking and P. A. Egelstaff, J. Phys. C **2**, 507 (1968).
[2] K. Sköld, J. M. Rowe, G. Ostrowski, and P. D. Randolph, Phys. Rev. A **6**, 1107 (1972).
[3] J.R.D. Copley and J. M. Rowe, Phys. Rev. A **9**, 1656 (1974).
[4] D. Levesque, L. Verlet, and J. Kurkijärvi, Phys. Rev. A **7**, 1690 (1973).
[5] A. Rahman, Phys. Rev. Lett. **32**, 52 (1974); Phys. Rev. A **9**, 1667 (1974).
[6] W. E. Alley, B. Alder, and S. Yip, Phys. Rev. A **27**, 3174 (1983).
[7] A. A. Van Well, P. Verkerk, L. A. de Graaf, J.-B. Suck, and J. R. D. Copley, Phys. Rev. A **31**, 3391 (1985), and references therein.
[8] A. A. Van Well and L. A. de Graaf, Phys. Rev. A **32**, 2396 (1985), and references therein.
[9] O. Söderström, U. Dahlborg, and W. Gudowsky, J. Phys. F **15**, L23 (1985), and references therein.
[10] J. Hubbard and J. L. Beeby, J. Phys. C **2**, 556 (1969).
[11] G. Dolling and V. F. Sears, Nucl. Instrum. Methods **106**, 419 (1973).
[12] H. Blank and B. Maier (unpublished).
[13] G. Bucher, Ph.D. thesis, Technische Universität München, 1984.
[14] V. F. Sears, Adv. Phys. **24**, 1 (1975).
[15] V. F. Sears, Chalk River Nuclear Laboratory Report No. AECL-8490, 1984 (unpublished).
[16] W. Ohse, *Handbook of Thermodynamic and Transport Properties of Alkali Metals* (Academic, Oxford, 1985).
[17] M. Shimoji and T. Itami, *Atomic Transport in Liquid Metals* (Trans Tech, Aedermannsdorf, Switzerland, 1986).
[18] T. Bodensteiner, Ph.D. Thesis, Technische Universität München, 1990.
[19] T. Soma and T. Satoh, J. Phys. F **10**, 1081 (1980).
[20] J. J. van Loef, Physica **75**, 115 (1974).
[21] J.R.D. Copley, P. Verkerk, A. A. van Well, and H. Fredrikze, Comput. Phys. Commun. **40**, 337 (1986), and references therein.
[22] S. W. Lovesey, J. Phys. C **4**, 3057 (1971).
[23] S. W. Lovesey, J. Phys. C **6**, 1857 (1973).
[24] H. Paalman and C. Pings, J. Appl. Phys. **33**, 2635 (1962).
[25] C. Morkel, Ph.D. Thesis, Technische Universität München, 1984.
[26] J. B. Boon and S. Yip, *Molecular Hydrodynamics* (McGraw-Hill, New York, 1980).
[27] A. A. Kugler, J. Stat. Phys. **8**, 107 (1973).
[28] N. K. Ailawadi, A. Rahman, and R. Zwanzig, Phys. Rev. A **4**, 1616 (1971).
[29] U. Balucani, R. Vallauri, and T. Gaskell, Phys. Rev. A **35**, 4263 (1987).
[30] A. Z. Akcazu and E. Daniels, Phys. Rev. A **2**, 962 (1970).
[31] K.-E. Larsson, M. Dzugutov, and W. Gudowsky, Nuovo Cimento D **12**, 559 (1990), and references therein.
[32] I. M. de Schepper, E.G.D. Cohen, and M. J. Zuilhof,

Phys. Lett. **101A**, 399 (1984).
[33] A. Rahman, *Inelastic Scattering of Neutrons* (IAEA, Wien, 1968), Vol. 1, p. 561.
[34] J. P. Hansen and I. R. McDonald, *Theory of Simple Liquids* (Academic, London, 1986).
[35] C. Morkel and T. Bodensteiner, J. Phys. Condens. Matter **2**, SA251 (1990).
[36] U. Bengtzelius, W. Götze, and A. Sjölander, J. Phys. Chem. **17**, 5915 (1984).